Response of Rubredoxin from *Pyrococcus furiosus* to Environmental Changes: Implications for the Origin of Hyperthermostability†

Silvia Cavagnero,‡ Zhi H. Zhou,§ Michael W. W. Adams,§ and Sunney I. Chan*,‡

Arthur Amos Noyes Laboratories of Chemical Physics, California Institute of Technology Pasadena, California 91125, and Department of Biochemistry and Center for Metalloenzyme Studies, University of Georgia, Athens, Georgia 30602

Received February 1, 1995; Revised Manuscript Received May 15, 1995⊗

ABSTRACT: The bases of the hyperthermostability of rubredoxin from *Pyrococcus furiosus* (RdPf) have been probed by structural perturbations induced by solution pH and ionic strength changes. Comparison of the solution behavior at pH 7 and pH 2, as probed by far- and near-UV circular dichroism, Trp fluorescence emission, 1-anilinonaphthalene-8-sulfonate (ANS) binding, and NMR spectroscopy, reveals the presence of only minimal structural variations at room temperature. At pH 2, the protein displays a surprising nearly native-like behavior at high ionic strength while, at low ionic strength, it is capable of strongly binding the hydrophobic probe ANS. All the secondary and tertiary structural features, including the environment of the hydrophobic core, appear to be intact regardless of pH and ionic strength. The apparent "melting" or denaturation temperature at pH 2, however, is 42 °C lower than at pH 7. This is attributed to the perturbation of many electrostatic interactions, including the disruption of all the ion pairs, which is complete at pH 2, as indicated by electrometric pH titrations. The implications of these findings for the origins of the hyperthermostability of rubredoxin are discussed.

The existence of life forms that live at elevated temperature and pressure is an open manifestation of nature's ingenuity in managing to support life even under the most adverse conditions. A variety of so-called hyperthermophilic microorganisms have been isolated in recent years (Stetter et al., 1990; Adams, 1990; Stetter, 1986) in the vicinity of both terrestrial and submarine hydrothermal vents. The majority of them are classified as *Archaea* (Woese et al., 1990) and thrive at temperatures up to 110 °C, the highest temperature known to be compatible with life. They are also the most slowly evolving or "primitive" of known organisms. Little is known of the novel biochemistry that must be required to sustain life above 100 °C. However, the quest for biomolecules displaying unusual and interesting physicochemical properties has recently led to the discovery and isolation of specific enzymes from these hyperthermophilic organisms. Among those that have been purified so far are proteases (Eggen et al., 1990; Cowan et al., 1987), redox proteins (Aono et al., 1989; Blake et al., 1991), hydrogenases (Bryant & Adams, 1989; Juszczak et al., 1991; Pihl & Maier, 1991), dehydrogenases (Robb et al., 1992), ferredoxin-dependent oxidoreductases (Mukund & Adams, 1990), DNA polymerases (Lundberg et al., 1991), and enzymes involved in carbohydrate metabolism (Koch & Zablowski, 1990; Constantino et al., 1990). These enzymes are composed of the regular 20 amino acids and display a thermal stability unknown to their mesophilic counterparts. Yet, sequence comparisons reveal no apparent striking differences. At this juncture, the origin of protein hyperthermostability (Flam, 1994; Adams & Kelly, 1992) is still an unsolved problem, and its understanding presents a great intellectual challenge to the chemist and the biochemist, not to mention its potentially enormous biotechnological impact (Kelly et al., 1994; Flam, 1994).

Several studies based on site-directed mutagenesis of nonthermophilic proteins have been able to show that even minimal stuctural variations are sufficient to cause some change in stability. T4 lysozyme, for instance, is a typical protein on which mutational analysis has been carried out extensively (Matsumura et al., 1989a,b; Nicholson et al., 1988; Matthews et al., 1987). However, relatively small variations have not, as yet, been sufficient to generate a hyperthermostable protein starting from a nonthermostable one. This immediately prompts the question of whether the structural/dynamic signatures of hyperthermostability are to be ascribed to a small number of specific noncovalent interactions, or more general rules exist that go beyond the identification of a few specific contributions.

We have started to address the problem by focusing our studies on the small (53 amino acids) hyperthermostable nonheme iron protein rubredoxin produced by the hyperthermophilic archaeon *Pyrococcus furiosus*. This microorganism, isolated by Fiala and Stetter (1986) in the vicinity of a mediterranean volcanic vent, grows under strictly anaerobic conditions and has an optimal growth temperature of 100 °C. Despite the fact that rubredoxin from *P. furiosus* (RdPf)[1] was isolated only recently (Blake et al., 1991), it is a remarkably well-characterized protein: its sequence is known (Blake et al., 1991), the crystal structures of both the oxidized

† This work was supported by NIH Grants GM 22432 (S.I.C.) and GM 50736 (M.W.W.A.) from the National Institute of General Medical Sciences, U.S. Public Health Service. Contribution No. 9039 from the Arthur Amos Noyes Laboratories of Chemical Physics.

* To whom correspondence should be addressed.
‡ California Institute of Technology.
§ University of Georgia.

⊗ Abstract published in *Advance ACS Abstracts,* July 15, 1995.

[1] Abbreviations: RdPf, rubredoxin from *Pyrococcus furiosus*; RdCp, rubredoxin from *Clostridium pasteurianum*; ANS, 1-anilinonaphthalene-8-sulfonate; $K_{d,app}$, apparent dissociation constant; CD, circular dichroism; T_m, melting temperature; ΔH_m, enthalpy of thermal unfolding; ΔC_p, heat capacity difference between the native and denatured state; $\Delta G(T)$, free energy difference between the native and denatured state at temperature T.

0006-2960/95/0434-9865$09.00/0

and the reduced forms have been solved (Day et al., 1992), and an NMR solution structure is available for the Zn-substituted protein (Blake et al., 1992a). The metal environment has been specifically probed by heteronuclear NMR experiments on various metal substituted forms (Blake et al., 1992b,c, 1994) and by X-ray absorption spectroscopy (George et al., 1992). The thermodynamics of stability has also been studied by differential scanning calorimetry (Klump et al., 1994).

The present study is designed to elucidate some of the factors that might be important in stabilizing a hyperthermophilic protein based on the structural perturbations induced by changes in solution pH, ionic strength, and temperature. The effects produced have been followed by Trp fluorescence emission, NMR, far- and near-UV circular dichroism (CD), 1-anilinonaphthalene-8-sulfonate (ANS) binding, and electrometric pH titrations. The surface charge density distribution has also been probed by surface potential calculations. All the experiments have been carried out on the high-spin Fe(III) form of RdPf. The implications of the results to the understanding of the hyperthermostability of RdPf and, possibly, of other proteins belonging to the same class are discussed.

MATERIALS AND METHODS

RdPf was isolated and purified as previously described (Blake et al., 1991). Protein concentrations were determined by using the previously published extinction coefficient at $\lambda = 280$ nm. High-purity ANS was purchased from Molecular Probes; 99.9% D_2O was purchased from Cambridge Isotopes.

Circular dichroism spectra were acquired with a JASCO 600 spectrophotometer using a water-jacketed 0.1 cm path quartz cell from Hellma in 10 mM phosphate buffer at either pH 2.0 or pH 7.2. When appropriate, the buffers also contained 1 M NaCl; after salt addition the pH was readjusted to the original value. RdPf concentration was 10−50 μM (far-UV CD) and 100 μM to 1 mM (near-UV CD). Temperature control for the CD experiment was achieved by connecting the cuvette to a water bath appropriately set to the desired temperature.

Fluorescence spectra were recorded with an SLM 4800 fluorometer. The Trp fluorescence emission spectra of RdPf were recorded at room temperature in a stirred fluorescence quartz cell. The sample was excited at 280 nm; the emission maximum was at 335 nm. The excitation bandwidth was set to 4 nm, and the emission bandwidth was set to 8 nm. The spectra were recorded in 20 or 40 mM phosphate buffers at variable pH, containing, when appropriate, 1 M NaCl. The excitation wavelength for the ANS emission spectra was 350 nm. The emission maximum varied between 510 and 480 nm, depending on the fraction of protein-bound ANS. Binding constants were determined by adding increasing amounts of ANS to RdPf solutions (3−4 μM). The fraction of bound ANS (α) was obtained by comparing the observed ANS fluorescence emission areas with the emission areas of quinine disulfate solutions (F_{qds}) having the same optical density (at 350 nm) as the ANS solutions (Kolb & Weber, 1975), according to the formula:

$$\alpha = (F_{obs} - F_0)/[(F_{qds}/A) - F_0] \quad (1)$$

where F_{obs} represents the observed ANS fluorescence in the presence of protein and F_0 is the fluorescence of ANS solutions of the same concentration but containing no protein. The constant A was determined via the relation:

$$A = F_{qds}/F_b \quad (2)$$

F_b represents the fluorescence of an ANS solution in the presence of protein at such a low ANS/protein ratio that virtually all the ANS is in bound form. The above procedure also has the advantage of internally correcting for inner filter effects due to the ANS. Apparent dissociation constants ($K_{d,app}$) were determined via nonlinear regression analysis. A plot of the average number of ANS molecules bound per protein molecule ($\langle n \rangle$) *vs* concentration of free ANS ([ANS]) was fit to the expression:

$$\langle n \rangle = N[\text{ANS}]/([\text{ANS}] + K_{d,app}) \quad (3)$$

The number of binding sites per protein molecule (N) was determined via linear regression analysis of Klotz plots (Klotz & Hunston, 1971).

UV−vis absorption spectra were recorded with a Hewlett-Packard 8452A single-beam diode array spectrophotometer. Spectra were obtained in water or aqueous buffer with a 1 cm quartz cuvette under constant stirring at 5 μM RdPf concentrations. Published values for the extinction coefficients of RdPf at the wavelengths of maximum absorption were used (Blake et al., 1991). The extinction coefficients of native RdPf in the UV−vis region are not temperature-dependent over the temperature range relevant to the present study (20−95 °C). However, they differ from the extinction coefficients of the unfolded form. In thermal denaturation experiments, unfolding was followed by monitoring the absorbance changes at 494 nm. The observed absorbance (F_{obs}) reflected the different populations of folded and unfolded forms at each individual temperature. The fraction of unfolded protein (X_u) was determined by using the formula:

$$X_u = (F_f - F_{obs})/(F_f - F_u) \quad (4)$$

F_f and F_u refer to the absorbance of the fully folded and fully unfolded protein, respectively. Apparent melting or denaturation temperature (T_m) values were derived as the temperature corresponding to $X_u = 0.5$. No curve fitting was employed, given the relatively high experimental error associated with the instrumentation used for temperature measurements. The temperature was controlled via a Haake D1 thermostated water bath connected to the compartment surrounding the cuvette housing. In thermal denaturation experiments, the temperature was increased at a rate of 2 °C/min. Temperature was monitored using a thermocouple probe connected to a Fluke 80TK module plugged into a multimeter. Readings were accurate to ±1 °C. The spectra were baseline corrected with the software Lab Calc.

Proton NMR spectra were acquired with a Bruker AMX-500 spectrometer. Protein concentrations for the NMR spectra were 1 mM; the experiments were performed either in 90:10 H_2O/D_2O or in D_2O. In this latter case, RdPf was concentrated in a Centricon 3 device (Amicon), diluted in D_2O, incubated at 37 °C for several hours, concentrated, and rediluted in D_2O; the procedure was repeated as necessary. The SUPERWEFT (Inubushi & Becker, 1983) experiment was performed at varying intervals of temperature up to 85 °C, using an interpulse delay of 50 ms, a recycle time of 0.5 s, and a sweep width of 250 ppm.

Electrometric pH titrations were performed with a pH meter from Radiometer Copenhagen Model PHM 93 equipped with a general purpose pHC2406 electrode. Titrations were

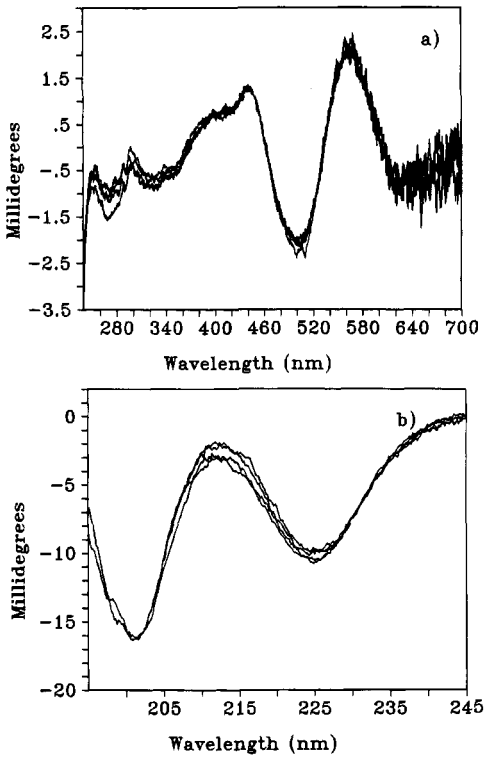

FIGURE 1: CD spectra of RdPf in the near-UV/visible (a) and far-UV (b) region. Each quadrant contains a superposition of the spectra of RdPf at pH 2.0 and pH 7.2, in the presence and absence of 1 M NaCl. The spectra have been recorded at room temperature.

performed under N_2 following previously described procedures (Tanford, 1962). Carefully standardized KOH and HCl solutions were necessary in order to obtain reliable results. RdPf solutions were concentrated with a Centricon 3 device (Amicon) and desalted using a PD10 column (Pharmacia), and KCl was added to a total ionic strength of 0.01. The solution was gently stirred through the duration of the whole experiment and acid/base additions were made while keeping conditions anaerobic. Data from calculations based on blank titrations have been subtracted from the experimental points for the protein-containing solutions. RdPf concentration was typically 0.3 mM.

The program GRASP (Nicholls et al., 1991) was used for surface potential calculations based on the Poisson–Boltzmann equation. The ionizable amino acids were assigned full or zero charge depending on the simulated pH; backbone carbons, nitrogens, and oxygens were assigned partial charges according to the CHARMM (Brooks et al., 1983) charge set. The crystal structures of RdPf (Day et al., 1992) and RdCp (Watenpaugh et al., 1979, 1980) have been used as the starting templates.

RESULTS

Circular Dichroism. Figure 1 shows a comparison of the CD spectra of RdPf in the far-UV, near-UV, and visible regions at pH 7 and 2 at variable ionic strengths. The far-UV CD (Figure 1b) probes the three-stranded antiparallel β-sheet environment that comprises about 30% of the RdPf primary sequence (Blake et al., 1991), while the CD in the near-UV and visible (Figure 1a), recorded between 240 and 700 nm, reflects the environment of the aromatic amino acids and the Fe(III) site. In all pH and ionic strength ranges examined, the spectra appear essentially unchanged, indicating that there are no significant changes in the secondary and tertiary structural elements under these conditions.

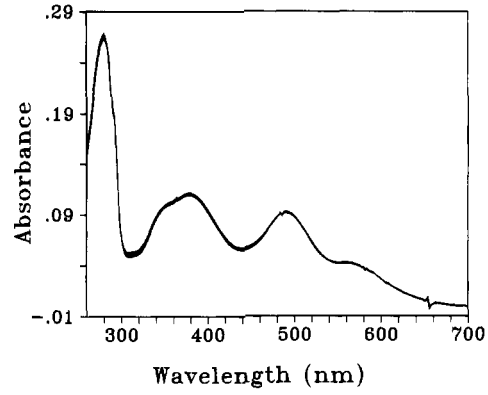

FIGURE 2: Absorption spectra of RdPf at room temperature in water at variable pH (pH values are 6.8, 5.4, 4.2, 3.8, 3.6, 3.3, 2.9, 2.4, 2.1, and 1.8).

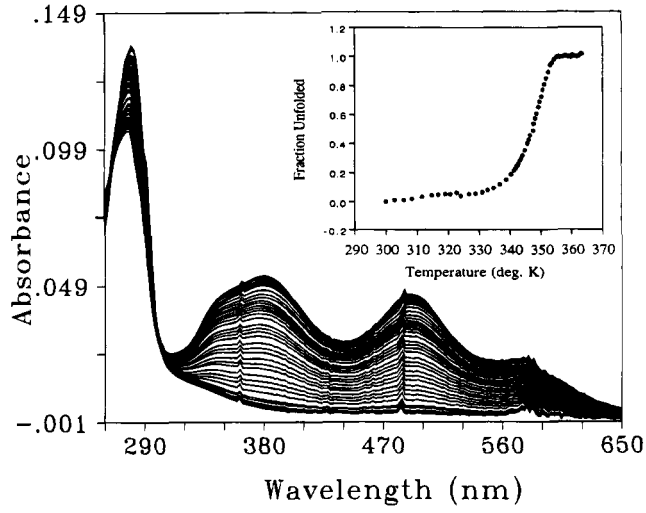

FIGURE 3: Thermal denaturation of RdPf in H_2O at pH 2.0 as followed by absorption spectroscopy. The corresponding denaturation curve is shown in the insert.

UV–Vis Absorption. The most informative feature of the absorption spectrum of oxidized RdPf comes from the signals with maxima centered at 380, 494, and 570 nm (Figure 2), which are attributed to ligand to metal charge-transfer transitions by analogy with the corresponding visible absorption bands of the nonthermophilic rubredoxin (Eaton & Lovenberg, 1973). At 25 °C, no spectral changes were observed between pH 6.8 and pH 1.8 (Figure 2), in agreement with the conclusions from the CD data.

RdPf undergoes thermal denaturation around 70 °C at pH 2. The protein absorption spectra as a function of temperature, and the corresponding thermal unfolding profile as followed by the decrease in absorbance at 494 nm, are shown in Figure 3. At pH 2 in H_2O, T_m was 71 °C. As expected, the unfolding was irreversible; i.e., upon cooling there was no increase in the visible absorption. In the presence of 1 M NaCl at pH 2 the melting temperature was higher (T_m = 80 °C).

Some unfolding experiments at low ionic strength were performed by first bringing the temperature of the solution to 71 °C and then lowering the pH stepwise. In this case it was found that the denaturation was 50% complete at pH 1.85.

Trp Fluorescence Emission. The intensity of the steady-state fluorescence emission of RdPf upon excitation at 280 nm (Trp) is rather weak due to the sulfur-coordinated iron center which, because of charge-transfer transitions, functions

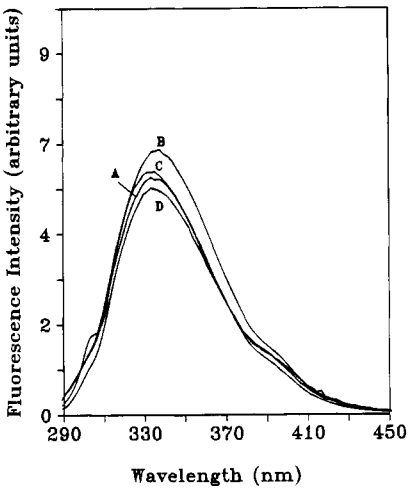

FIGURE 4: Fluorescence emission spectra of RdPf upon excitation at 280 nm. Buffers are as follows: 20 mM phosphate and 1 M NaCl, pH 2.0 (A), 20 mM phosphate, pH 2.0 (B), 20 mM phosphate and 1 M NaCl, pH 7.0 (C), and 20 mM phosphate, pH 7.0 (D). The spectra have been recorded at 24 °C.

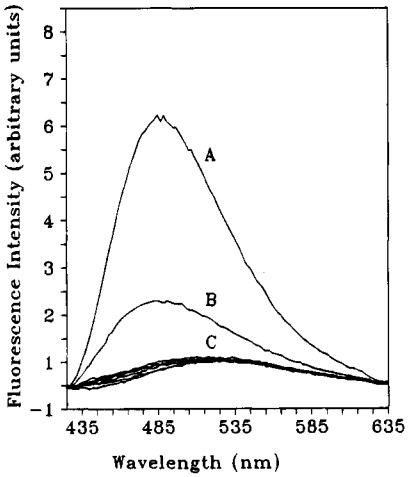

FIGURE 5: ANS fluorescence emission spectra in the absence and presence of RdPf at variable pH and ionic strength values: ANS + RdPf, pH 2.0 (A); ANS + RdPf and 1 M NaCl, pH 2.0 (B); ANS + RdPf, pH 7.0 (C); ANS + RDPf and 1 M NaCl, pH 7.0 (C); ANS, pH 2.0 (C); ANS, pH 7.0 (C). Phosphate buffer (40 mM) has been used. ANS concentration is 0.8 μM in all spectra. Buffer blanks have been subtracted. All the spectra have been recorded at 24 °C.

as an inner filter, thereby decreasing the effective Trp fluorescence quantum yield. Although this decreases sensitivity, Trp fluorescence emission data of RdPf show that the Trp environment is relatively insensitive to pH and ionic strength. For example, Figure 4 compares the Trp emission at pH 2 and 7.2, room temperature, in various buffers and ionic strengths, demonstrating the exceptional resistance of RdPf to pH extremes when compared to the typical behavior of nonthermophilic proteins.

ANS Binding. ANS is a polycyclic aromatic fluorescent probe that interacts with proteins whose hydrophobic sites are, to some extent, solvent-exposed (Semisotnov et al., 1991). It has been used extensively to probe the molten globular states (Kuwajima, 1989) of proteins; we have applied this approach to RdPf to probe the overall folding of the protein at low pH. Figure 5 shows that, at pH 2, room temperature, and low ionic strength, the quantum yield for the ANS fluorescence emission increases dramatically upon addition of RdPf to the solution in nearly equimolar amounts.

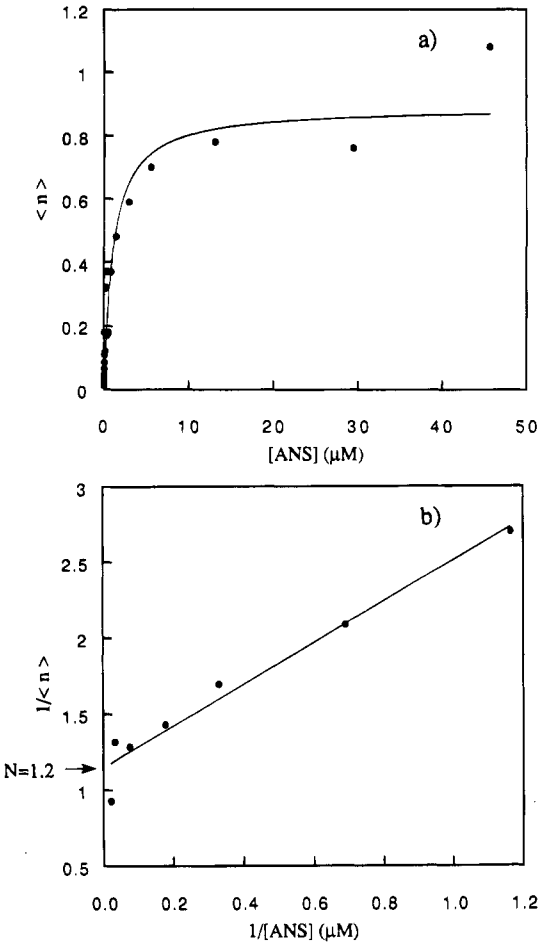

FIGURE 6: Saturation curve (a) of RdPf at pH 2.0 upon addition of variable amounts of ANS. RdPf concentration is 3.8 μM. $\langle n \rangle$ is the average number of ANS molecules bound per protein molecule; [ANS] represents the free ANS concentration. Klotz plot (b) of ANS binding to RdPf at pH 2.0. The total number of binding sites per protein molecule (N) derived from curve fitting is indicated on the figure.

Analysis of the concentration dependence of ANS binding yields a $K_{d,app}$ of 1.1 μM (Figure 6a). The Klotz plot (Klotz & Hunston, 1971) shown in Figure 6b is consistent with a 1:1 ANS to protein binding stoichiometry (N = 1.2). However, the binding takes several hours to reach equilibrium. At pH 2, the ANS binding becomes weaker at high ionic strength ($K_{d,app}$ = 37 μM), and it is completely suppressed at pH 7, regardless of the ionic strength.

NMR Spectroscopy. Proton NMR spectra of RdPf were recorded at pH ranging from 8 to 2. The 1D ^{1}H NMR spectrum changes only slightly upon lowering the pH. Although the spectral changes due to individual peaks are hard to follow, careful inspection indicates that some lines undergo extensive broadening without chemical shift changes. We emphasize that the 1D NMR spectrum has revealed no overall variations in chemical shift dispersion over the pH range 8−2. Furthermore, the observed spectral changes were completely reversible.

The presence of high-spin Fe(III) in the oxidized RdPf introduces a hyperfine and pseudohyperfine chemical shift contribution to the proton resonances (Bertini & Luchinat, 1986). The former only affects protons four or five bonds removed from the iron site; these protons, due to the high magnetic moment of high-spin Fe(III), undergo extensive line broadening. The pseudohyperfine contribution to the chemical shift is dipolar in nature, and in the case of axially

symmetric systems, it is proportional to $(g_{\parallel} - g_{\perp})$, which vanishes in a perfectly tetrahedral system. According to the crystal structure of RdPf (Day et al., 1992), the S−Fe−S bond angles deviate from perfect tetrahedral symmetry by less than 6°, and the Fe−S bonds are all of nearly equal length, ranging from 2.27 to 2.31 Å. Low-temperature EPR studies on rubredoxin from *Pseudomonas oleovorans* revealed dispersion arising from zero-field splitting, with $D \approx 1.51$ cm^{-1} and $E/D = 0.28$ (Peisach et al., 1971). This result has been interpreted by Peisach and co-workers in terms of "substantial" rhombic distortion. However, at ambient temperatures, we expect rapid relaxation among the zero-field states, in which case any subtle effects of the zero-field splitting on the proton chemical shifts are expected to be small, if not negligible. This should be, particularly, the case here, since D is small. If so, the pseudocontact shifts should be governed by any intrinsic anisotropy in the electron Zeeman interaction. Judging from the low-temperature EPR data, where signals from at least two pairs of the zero-field levels are observed, we have concluded that $\Delta g \leq 0.01$. This implies that the pseudocontact contributions to the observed proton NMR chemical shifts of oxidized RdPf should be minimal. In support of this, proton NMR analysis of oxidized rubredoxin from *Clostridium pasteurianum* (RdCp) did not reveal any resonance out of the diamagnetic envelope at 200 MHz (Phillips et al., 1970), and some very broad peaks only slightly downfield to the diamagnetic envelope were noted when the analysis was performed at 470 MHz (Krishnamoorthi et al., 1986); we have found similar results for RdPf after extensive accumulation with the SUPERWEFT pulse sequence (data not shown). As a consequence, most of the chemical shift values of Zn-substituted RdPf (Blake et al., 1991) should be very similar to those of the oxidized native RdPf.

In the case of RdPf, the ^{1}H NMR resonance most diagnostic of the tertiary folding of the protein is the peak at −1.61 ppm (at 27 °C) which has been assigned to Leu 32 δCH_3 in the Zn-substituted RdPf. This methyl group has an average distance of 12.5 Å from the metal. This, together with the above discussion, implies negligible pseudocontact contributions to the observed proton chemical shift of this resonance in the native RdPf; the assignment is therefore extended to the native oxidized RdPf. This signal is an NMR probe of the hydrophobic core. Careful scrutiny of the spectral data shows that this resonance does not undergo any chemical shift change when the pH is lowered to 2.

Electrometric pH Titrations. Electrometric pH titrations are the most direct and unequivocal technique to detect the number of groups that become ionized as the pH changes. The pH titration curve of RdPf at low ionic strength is shown in Figure 7. RdPf has several ionizable groups: 7 Asp, 6 Glu, and 5 Lys out of 53 residues. The titration end point at low pH is clearly marked as the curve flattens toward pH 2. Proton consumption and group counting shows that, upon going from pH 7 to pH 2, all the Asp, Glu, and the carboxyl terminus have been protonated. The titration end points of individual residues are not resolved, but this is typical of the pH titration curves of charged polymers. The curve does not differ, in its general features, from the corresponding curves of common proteins.

Surface Potential Calculations. The surface potential of RdPf has been calculated with the software GRASP (Nicholls et al., 1991). The charge files used are intended to simulate the observed protonation state of the protein at pH 7 and

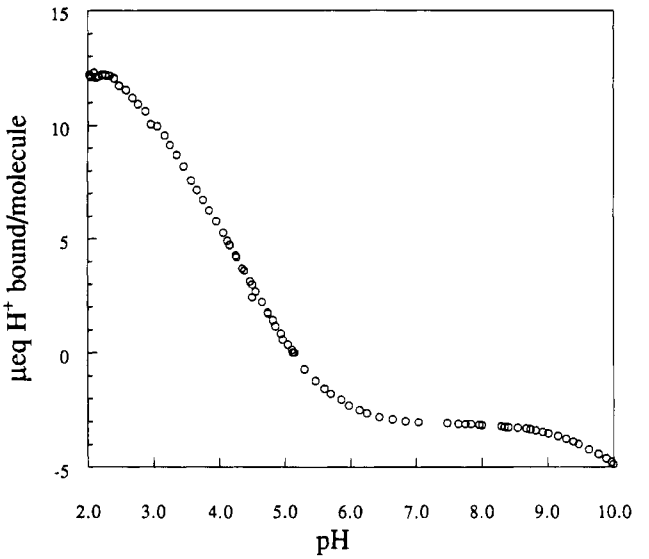

FIGURE 7: Electrometric pH titration curve of RdPf.

pH 2. The calculations illustrate the surface charge density distribution and its changes as a function of pH. Figure 8a simulates the protonation state of RdPf at pH 7 and shows that all the charge density due to the positively and negatively charged amino acids resides on the surface of the protein. Furthermore, most of the negatively charged functionalities (Asp, Glu, and carboxyl terminus) are distributed on one side of the molecule (see image on the left of Figure 8a). Interestingly, the five positively charged amino acids (Lys) and the amino terminus are also clustered on the same side of the molecule allowing for a number of ion pairs to be formed, including those between Glu 14 and the amino terminus and between Glu 47/Glu 49 and Lys 6. These are the ion pairs that have been proposed to be unique to RdPf (Day et al., 1992).

Figure 9 illustrates the surface charge density distribution of the rubredoxin from *C. pasteurianum*, a mesophilic organism. It is noted that the negatively charged functionalities are distributed much more evenly than in the case of RdPf. The four Lys and the amino terminus, on the other hand, are clustered on one side of the molecule (see upper region of the images of Figure 9). This results, as in the case of RdPf, in a greater concentration of ion pairs on one side of the molecule.

The surface charge density distribution of RdPf at pH 2 is illustrated in Figure 8b. Since the simulated pH is considerably lower than the isoelectric point, the protein appears, as expected, mostly positively charged. Furthermore, there appears to be an area of particularly highly positive surface potential in the region comprised among the amino terminus and the amino groups of Lys 28 and Lys 50. This region is a strong candidate for the site of ANS binding at pH 2, as further discussed in the next section.

DISCUSSION

The phenomenon of protein hyperthermostability, i.e., the ability of proteins from hyperthermophilic organisms to be in their folded state at temperatures near 100 °C, is not well understood at present, and its study is made more challenging by the experimental problems associated with working at temperatures near and above 100 °C in aqueous buffer. In addition, the phenomenon may also depend on contributions from unfolded forms of the proteins which are hard to examine experimentally (Dill & Shortle, 1991). The origins

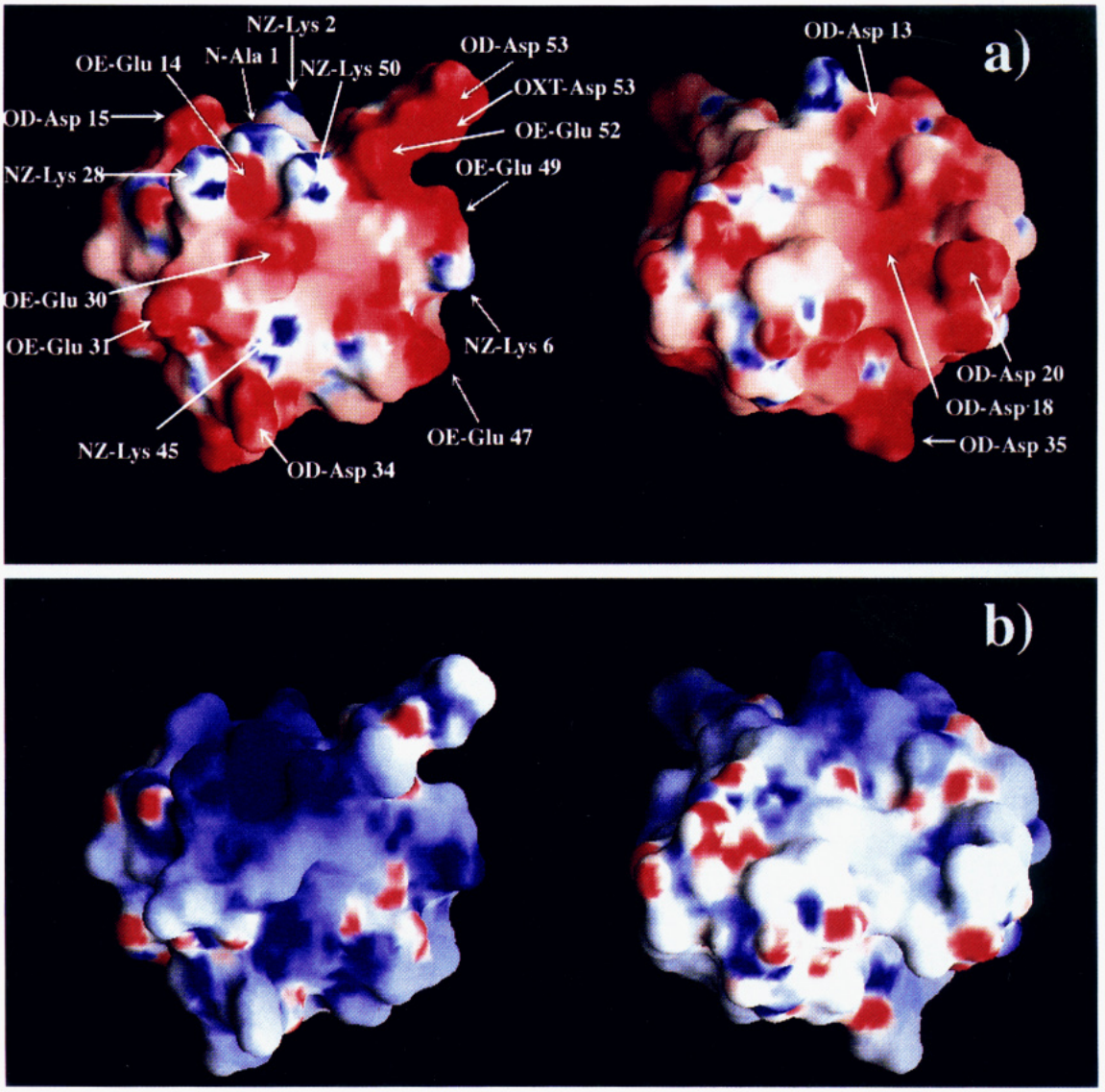

FIGURE 8: Surface potential images of RdPf at pH 7 (a) and pH 2 (b). For each pH value, the protein is represented by two images that correspond to opposite sides of the molecule. Surfaces are color-coded as follows: red, white, and blue represent regions of negative, zero, and positive charge density, respectively. All the negatively and positively charged groups have been labeled in part a. The prefixes of the amino acid labels represent the following: OD and OE, oxygens of the side-chain carboxylates of Asp and Glu, respectively; NZ, nitrogen of the side-chain amino group of Lys; OXT, oxygens of the carboxyl terminus; N, nitrogen of the amino terminus.

of thermal stability may be addressed by the comparison of the native and perturbed states of a protein at ambient temperature, and more quantitative information may be gained by evaluating all the parameters in the relevant thermodynamic cycle. This is feasible provided that all the steps involved are reversible. Destabilization of a protein at a given temperature by a chemical or physical perturbation, though, does not necessarily imply a decrease in T_m; and conversely, a lower T_m is not a sufficient condition to guarantee decreased stability at room temperature. This arises from the intrinsic shape of the stability curve which is determined, in turn, by the enthalpy difference between the folded and unfolded states at $T = T_m$ (ΔH_m), the heat capacity difference between the two states (ΔC_p), and T_m (Becktel & Schellman, 1987). For a two-state process and for ΔC_p independent of temperature, the stability curve is represented by

$$\Delta G(T) = \Delta H_m(1 - T/T_m) - \Delta C_p(T_m - T + T \ln(T/T_m)) \quad (5)$$

However, when a protein is examined under different experimental conditions, such as arising from pH variations, one can assume that the free energy of stabilization at ambient temperature [ΔG(25 °C)] is proportional to T_m, provided some conditions are met. The fact that the enthalpy of thermal unfolding (ΔH_m) and the melting temperature (T_m) at low pH are generally lower than that at neutral pH and the relative independence of ΔC_p on pH usually lead to a stability curve at pH close to neutral which lies above the curve at lower pH. As long as one deals with proteins which satisfy the above mentioned conditions, one can then make comparisons between melting temperatures and qualitatively relate them to structural features at room temperature. However, it is necessary to keep in mind that the validity of these assumptions in the case of hyperthermophilic proteins would have to be experimentally verified by accurate calorimetric studies. In particular, it has been seen that, for most of the nonthermophilic proteins that have been studied by calorimetry, ΔC_p is, to a first approximation, temperature independent. However, recent evidence coming from the study of BPTI (Makhatadze et al., 1993) shows that ΔC_p decreases considerably at higher temperatures, introducing some asymmetry in the stability curve. This may also turn

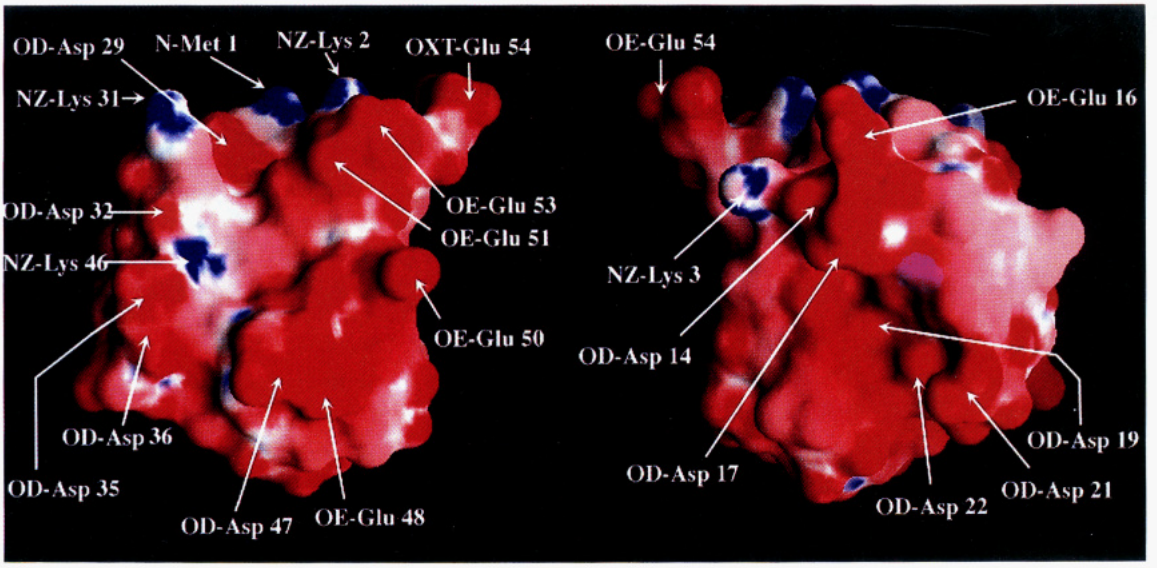

FIGURE 9: Surface potential images of RdCp at pH 7. The protein is represented by two images that correspond to opposite sides of the molecule. Surfaces are color-coded as in Figure 8. All the negatively and positively charged groups have been labeled. The prefixes of the amino acid labels follow the nomenclature of Figure 8.

out to be true for hyperthermophilic proteins. Under the experimental conditions of this study, the thermal denaturation of RdPf turned out to be irreversible. We postulate that this is due to processes that take place at high temperature upon denaturation. However, as long as the heating rates are not too slow compared with the rate of the irreversible step, a qualitative comparison of experimental melting temperatures (T_ms) that are sufficiently far apart is meaningful.

The totality of the experimental evidence presented herein from absorption spectroscopy, CD, NMR, and Trp fluorescence emission indicates that RdPf is still folded at pH 2. Both the secondary structure of the molecule as well as the environments around the metal and the aromatic amino acids including Trp 3, Trp 36, and Leu 32 remain unchanged between pH 7 and pH 2. These observations document the exceptional resistance of the protein to very low pH conditions. Although experiments at even lower pH were undertaken as part of this study, these results are not reported here as the observations obtained at pH lower than 2 may be compromised by peptide bond hydrolysis.

The ANS binding data have allowed us to refine our picture of the structure of RdPf by revealing that, at pH 2 and low ionic strength, a folded form with enhanced accessibility to hydrophobic groups is generated. This structure differs from what has traditionally been called a molten globule (Kuwajima, 1989), since there is no substantial disruption of tertiary interactions as probed by near-UV circular dichroism and absorption spectroscopy. Moreover, the chemical shift dispersion in the proton NMR spectrum remains fully preserved. This low-pH pseudo-native state of RdPf is unique in that it is even more structured than the recently discovered highly ordered molten globular forms of interleukin-4 (Redfield et al., 1994). In this case, the ANS binding was accompanied by changes in the near-UV CD spectrum, even though a small change in the proton chemical shift dispersion was not observed.

In the present case of RdPf at pH 2, the ANS binding was found to be greatly diminished at 1 M NaCl. This result suggests that the structural change that causes ANS binding is, at least partially, of electrostatic origin. In order to study whether the surface charge density distribution might have any relationships to hyperthermostability and the observed features of ANS binding, we have calculated the surface potential of RdPf according to the Poisson−Boltzmann equation. The amino acid charges at either pH 7 or pH 2, consistent with the results from the pH titration data (see below), have been incorporated into the calculations. The overall increased density of positive charge at low pH, a mere consequence of the protonation state of RdPf and its low isoelectric point, is surprisingly accompanied by the creation of a well-defined region of extremely high and positive charge density (see upper region of left image of Figure 8b). We propose that this is the site responsible for the initial interaction of the negatively charged ANS with the protein. This idea is supported by the observed 1:1 binding stoichiometry and the ionic strength dependence of the binding. We propose that this event is followed by the penetration of ANS into the hydrophobic core of the protein. The accessibility of the hydrophobic core might be explained in terms of a slight "opening" of the protein surface driven by the elevated charge repulsion at the putative binding site. The high surface charge density at pH 7 makes RdPf very hydrophilic and therefore explains its high water solubility. The elevated positive surface charge density at low pH is also consistent with the increased thermal stability at higher ionic strengths which was observed under those conditions. In the absence of salt bridges, the dominant contribution to the electrostatic free energy comes from the positive surface charge, which can be effectively shielded in the presence of salt. This may, in fact, be a simple trick played by nature in order to increase the thermal stability of soluble proteins whose habitat has very high intracellular salt concentrations. It has been found, for instance, that elevated potassium salt concentrations (about 0.5 M) are present in the cells of the archaeon *Pyrococcus woesei* (Scholz et al., 1992; Zwickl et al., 1990).

The pH titration data at low ionic strength indicate that at pH 2 all the titratable groups have been protonated. This implies that the low pH state of RdPf no longer has any ion pairs at pH 2. This is an important observation, since it shows that ion pairs do not play a significant role in the remarkable thermal stability of the pH 2 form of RdPf. Thermal denaturation data do indicate that the pH 2 form of

RdPf has a lower apparent T_m than a pH 8.25 state (Klump et al., 1994; H. H. Klump, unpublished results) by 42 °C. The observed apparent decreased thermostability at low pH may well be accounted for by the disruption of all the ion pairs observed in RdPf at the higher pH: Glu 14 to Ala 1 (amino terminus), Glu 30 (and/or Asp 34) to Lys 28 and Lys 45, and Glu 47 (and/or Glu 49) to Lys 6. Additionally, Glu 14 is also thought to form a hydrogen bond with the indole nitrogen of Trp 3. However, protonation of the carboxylate of Glu 14, which has definitely occurred at pH 2, does not result in sizable changes in the Trp fluorescence emission profile, which is believed to be a sensitive probe of the Trp environment.

The correlation between decrease in thermostability and disruption of ion pairs suggests that these ion pairs play some role in making a protein hyperthermostable. However, our experiments have shown that RdPf is folded at room temperature and pH 2. This is a remarkable observation, as typical proteins at pH 2 (Privalov, 1979), including metalloproteins such as cytochrome *c* (Goto et al., 1990; Stellwagen & Babul, 1975; Babul & Stellwagen, 1972), zinc finger peptides (Krizek et al., 1991), and lactoferrin and transferrin (Mazurier & Spik, 1980), are either denatured or in a molten globular state. A known exception is given by some disulfide-containing proteins such as lysozyme (Privalov & Khechinashvili, 1974) and bovine pancreatic trypsin inhibitor (Makhatadze et al., 1993). However, it is generally believed that their high thermal and pH stability is mainly due to the presence of the disulfides, which provide a covalent structural constraint. Upon reduction, these proteins become fully unfolded at pH 2 and room temperature (Privalov et al., 1989). RdPf, as all the rubredoxins produced by nonhyperthermophilic organisms, has no disulfides. On the other hand, here the four conserved cysteine sulfurs are engaged in tetrahedral iron coordination. This is a common feature of all the rubredoxins, and to a first approximation, one would expect the free energy contribution given by the tetracoordinate iron to be fairly similar for different species. It is possible that the high resistance to low pH is a common characteristic of rubredoxins and it is related to the presence of the iron−sulfur core, rather than being a peculiar property of RdPf. Indirect evidence about mesophilic rubredoxins comes from a report that RdCp is present as a distribution of holo and apo forms when analyzed by electrospray ionization mass spectrometry under conditions when the protein exists as a positive ion (pH = 2.4; Petillot et al., 1993). The fact that the apparent "melting" temperature of RdPf is lower at pH 2 than at pH 8.25 suggests that ion pairs play a role in the thermal stability. However, their contribution cannot be dominant over other forces since the protein still has an unusually high T_m at pH 2. The observed apparent T_m is, in fact, higher than that of typical non-disulfide containing mesophilic proteins, including metalloproteins, under low pH conditions.

Analysis of Figure 8a shows that, at neutral pH, both the negative and positive charges of RdPf are concentrated on one side of the molecule, allowing all the above cited ion pairs to be clustered in close proximity of each other. The nonthermophilic rubredoxin that has been analyzed (RdCp) also has a number of ion pairs relatively close to each other (Figure 9). However, here the distribution of negative charge density is more uniform across the whole protein surface. It is not possible, at this point, to draw any definite conclusion from the comparison of the charge density distribution of the two proteins.

The above conjectures are consistent with the proposal based on mutation studies on lysozyme from bacteriophage T4 (Daopin et al., 1991) that the enthalpic gain realized by the addition of an ion pair to a mesophilic protein is, at least partially, counterbalanced by the entropic loss due to decreased degrees of freedom of the side chain, with resulting small free energy advantage. More generally, the fact that electrostatic interactions are not the dominant force of protein folding has been discussed previously (Dill, 1990). It could well be that the importance of ion pairing in hyperthermophilic protein stability has been overemphasized in the past, at least in the sense that these interactions are not the dominant factors affecting hyperthermostability. The present study represents one of the first attempts to address this issue experimentally. However, these thermodynamic considerations may not pertain to the situation under study here.

In the course of this work, we have noted that the denaturation of RdPf is irreversible. The denaturation process may be described by the following general kinetic model:

$$N \underset{k_{-1}}{\overset{k_1}{\rightleftharpoons}} N^* \underset{k_{-2}}{\overset{k_2}{\rightleftharpoons}} U \xrightarrow{k_3} A \qquad (6)$$

where N represents the native state, N* is an intermediate, U is the unfolded form, and A is a possible stable unfolded-like state to account for additional processes (aggregation or chemical modification) if the overall unfolding event is irreversible. A hyperthermophilic metalloprotein such as RdPf might undergo disruption of all the noncovalent interactions not involving the iron in the first step and disruption of the iron−sulfur interactions in the second step. If these steps are sufficiently rapid at temperatures approaching T_m, the concentration of N* may be sufficiently negligible that N ⇌ U approximates a two-state process, provided that the unfolding is reversible (i.e., k_3 is small). The difference between mesophilic and thermophilc rubredoxins could merely reflect the magnitudes of the rate constants k_1 and k_2. For instance, k_1 could be smaller due to a much higher kinetic barrier for the first step in the case of RdPf. In this case the thermal transition would be under kinetic control; i.e., it would be characterized by a relatively high kinetic or activation barrier that could only be "crossed" to a significant extent at temperatures close to the apparent T_m. It is possible that lowering the solution pH causes the height of this barrier to go down. This would result in a lower apparent T_m. Such a scenario could arise from the disruption of the structural constraints exerted by the ion pairs. Nothing could be said at this point about the height of the kinetic barrier associated with the second step, except that it is not exceedingly high for RdPf at low pH.

The unfolding experiments undertaken in the present study were typically performed by bringing the pH to 2 and then heating the protein solution. On the other hand, when we performed the experiments by first bringing the temperature up to T_m and then lowering the pH stepwise, we noticed some hysteresis (see Results section). These observations are consistent with the nature of the denaturation mentioned above.

The data obtained here provide the first example of a detailed characterization of the highly ordered low pH state of a hyperthermophilic protein. The results obtained should have implications for the understanding of the origins of the

hyperthermostability of RdPf. Ion pairing seems to play a role, but it does not appear to be the main contributing factor to the hyperthermostability. This conclusion may not be true for RdPf alone and may apply to other thermophilic proteins as well. Contributions due to other forces need to be examined and should shed further light on this intriguing problem.

ACKNOWLEDGMENT

We thank Professor Pamela J. Bjorkman for the use of the program GRASP and Professor Douglas C. Rees for helpful discussion on this study.

REFERENCES

Adams, M. W. W. (1990) *FEMS Microbiol. Rev. 75*, 219−238.
Adams, M. W. W. (1993) *Annu. Rev. Microbiol. 47*, 627−658.
Adams, M. W. W., & Kelly, R. M. (1992) in *Biocatalysis at Extreme Temperatures, Enzyme Systems Near and Above 100 °C* (Adams, M. W. W., & Kelly, R. M., Eds.) pp 1−3, ACS Symposium Series 498, American Chemical Society, Washington, DC.
Aono, S., Bryant, F. O., & Adams, M. W. W. (1989) *J. Bacteriol. 171*, 3433−3439.
Babul, J., & Stellwagen, E. (1972) *Biochemistry 11*, 1195−1200.
Becktel, W. J., & Schellman, J. A. (1987) *Biopolymers 26*, 1859−1877.
Bertini, I., & Luchinat, C. (1986) in *NMR of Paramagnetic Molecules in Biological Systems*, pp 19−46, The Benjamin/Cummings Publishing Co., Inc., Menlo Park, CA.
Blake, P. R., Park, J.-B., Bryant, F. O., Aono, S., Magnuson, J. K., Eccleston, E., Howard, J. B., Summers, M. F., & Adams, M. W. W. (1991) *Biochemistry 30*, 10885−10895.
Blake, P. R., Park, J.-B., Zhou, Z. H., Hare, D., Adams, M. W. W., & Summers M. F. (1992a) *Protein Sci. 1*, 1508−1521.
Blake, P. R., Lee, B., Summers, M. F., Adams, M. W. W., Park, J.-B., Zhou, Z. H., & Bax, A. (1992b) *J. Biomol. NMR 2*, 527−533.
Blake, P. R., Park, J.-B., Adams, M. W. W., & Summers, M. F. (1992c) *J. Am. Chem. Soc. 114*, 4931−4933.
Blake, P. R., Lee, B., Summers, M. F., Park, J.-B., Zhou, Z. H., & Adams, M. W. W. (1994) *New J. Chem. 18*, 387−395.
Brooks, B. R., Bruccoleri, R. E., Olafson, B. D., States, D. J., Swaminathan, S., & Karplus, M. (1983) *J. Comput. Chem. 4*, 187−217.
Bryant, F. O., & Adams, M. W. W. (1989) *J. Biol. Chem. 264*, 5070−5079.
Constantino, H. R., Brown, S. H., & Kelly, R. M. (1990) *J. Bacteriol. 172*, 3654−3660.
Cowan, D. A., Smolenski, K. A., Daniel, R. M., & Morgan, H. W. (1987) *Biochem. J. 247*, 121−133.
Daopin, S., Nicholson, H., Baase, W. A., Zhang, X. J., Wozniak, J. A., & Matthews, B. W. (1991) *Ciba Found. Symp. 161*, 52−62.
Day, M. W., Hsu, B. T., Joshua-Tor, L., Park, J.-B., Zhou, Z. H., Adams, M. W. W., & Rees, D. C. (1992) *Protein Sci. 1*, 1494−1507.
Dill, K. A. (1990) *Biochemistry 29*, 7133−7155.
Dill, K., & Shortle, D. (1991) *Annu. Rev. Biochem. 60*, 795−825.
Eaton, W. A., & Lovenberg, W. (1973) in *Iron-Sulfur Proteins* (Lovenberg, W., Ed.) pp 131−162, Academic Press, New York and London.
Eggen, R., Geerling, A., Watts, J., & de Vos, W. M. (1990) *FEMS Microbiol. Lett. 71*, 17−20.
Fiala, G., & Stetter K. O. (1986) *Arch. Microbiol. 145*, 56−61.
Flam, F. (1994) *Science 265*, 471−472.
George, S. J., van Elp, J., Chen, J., Ma, Y., Chen, C. T., Park, J.-B., Adams, M. W. W., Searle, B. G., de Groot, F. M. F., Fuggle, J. C., & Cramer, S. P. (1992) *J. Am. Chem. Soc. 114*, 4426−4427.
Goto, Y., Calciano, L. J., & Fink, A. L. (1990) *Proc. Natl. Acad. Sci. U.S.A. 87*, 573−577.
Inubushi, T., & Becker, E. D. (1983) *J. Magn. Reson. 51*, 128−133.
Juszczak, A., Aono, S., & Adams, M. W. W. (1991) *J. Biol. Chem. 266*, 13834−13841.
Kelly, R. M., Baross, J. A., & Adams, M. W. W. (1994) *Chem. Br. 30* (7), 555−558.
Klotz, I. M., & Hunston, D. L. (1971) *Biochemistry 10*, 3065−3069.
Klump, H. H., Adams, M. W. W., & Robb, F. T. (1994) *Pure Appl. Chem. 66* (3), 485−489.
Koch, R., & Zablowski, P. (1990) *FEMS Microbiol. Lett. 71*, 21−26.
Kolb, D. A., & Weber, G. (1975) *Biochemistry 14*, 4471−4476.
Krishnamoorthi, R., Markley, J. L., Cusanovich, M. A., & Przysiecki, C. T. (1986) *Biochemistry 25*, 50−54.
Krizek, B. A., Amann, B. T., Kilfoil, V. J., Merkle, D. L., & Berg, J. M. (1991) *J. Am. Chem. Soc. 113*, 4518−4523.
Kuwajima, K. (1989) *Proteins: Struct., Funct., Genet. 6*, 87−103.
Lundberg, K. S., Shoemaker, D. D., Short, J. M., Sorge, J. A., Adams, M. W. W., & Mathur, E. (1991) *Gene 108*, 1−6.
Makhatadze, G. I., Kim, K.-S., Woodward, C., & Privalov, P. L. (1993) *Protein Sci. 2*, 2028−2036.
Matsumura, M., Becktel, W. J., Levitt, M., & Matthews, B. W. (1989a) *Proc. Natl. Acad. Sci. U.S.A. 86*, 6562−6566.
Matsumura, M., Signor, G., & Matthews, B. W. (1989b) *Nature 342*, 291−293.
Matthews, B. W., Nicholson, H., & Becktel, W. J. (1987) *Proc. Natl. Acad. Sci. U.S.A. 84*, 6663−6667.
Mazurier, J., & Spik, G. (1980) *Biochim. Biophys. Acta 629*, 399−408.
Mukund, S., & Adams, M. W. W. (1990) *J. Biol. Chem. 265*, 11508−11516.
Nicholls, A., Sharp, K., & Honig, B. (1991) in *Proteins: Struct., Funct., Genet. 11*, 281−296.
Nicholson, H., Becktel, W. J., & Matthews, B. W. (1988) *Nature 336*, 651−656.
Peisach, J., Blumberg, W. E., Lode, E. T., & Coon, M. J. (1971) *J. Biol. Chem. 246*, 5877−5881.
Petillot, Y., Forest, E., Mathieu, I., Meyer, J., & Moulis, J.-M. (1993) *Biochem. J. 296*, 657−661.
Phillips, W. D., Poe, M., Weiher, J. F., Mc Donald, C. C., & Lovenberg, W. (1970) *Nature 227*, 574−577.
Pihl, T. D., & Maier, R. J. (1991) *J. Bacteriol. 173*, 1839−1844.
Privalov, P. L. (1979) *Adv. Protein Chem. 33*, 167−241.
Privalov, P. L., & Khechinashvili, N. N. (1974) *J. Mol. Biol. 86*, 665−684.
Privalov, P. L., Tiktopulo, E. I., Venyaminov, S. N., Griko, Y. V., Makhatadze, G. I., & Khechinashvili, N. N. (1989) *J. Mol. Biol. 205*, 737−750.
Redfield, C., Smith, R. A. G., & Dobson, C. M. (1994) *Nature Struct. Biol. 1*, 23−29.
Robb, F. T., Park, J.-B., & Adams, M. W. W. (1992) *Biochim. Biophys. Acta 1120*, 267−272.
Scholz, S., Sonnenbichler, J., Schäfer, W., & Hensel, R. (1992) *FEBS Lett. 306*, 239−242.
Semisotnov, G. V., Rodionova, N. A., Razgulyaev, O. I., Uversky, V. N., Gripas, A. F., & Gilmanshin, R. I. (1991) *Biopolymers 31*, 119−128.
Stellwagen, E., & Babul, J. (1975) *Biochemistry 14*, 5135−5140.
Stetter, K. O. (1986) in *The Thermophiles: General, Molecular, and Applied Microbiology* (Brock, T. D., Ed.) pp 39−74, John Wiley, New York.
Stetter, K. O., Fiala, G., Huber, G., Huber, R., & Segerer, G. (1990) *FEMS Microbiol. Rev. 75*, 117−124.
Tanford, C. (1962) *Adv. Protein Chem. 17*, 69−165.
Watenpaugh, K. D., Sieker, L. C., & Jensen, L. H. (1979) *J. Mol. Biol. 131*, 509−522.
Watenpaugh, K. D., Sieker, L. C., & Jensen, L. H. (1980) *J. Mol. Biol. 138*, 615−633.
Woese, C. R., Kandler, O., & Wheelis, M. L. (1990) *Proc. Natl. Acad. Sci. U.S.A. 87*, 4576−4579.
Zwickl, P., Fabry, S., Bogedain, C., Haas, A., & Hensel, R. (1990) *J. Bacteriol. 172*, 4329−4338.

BI9502194